Calculated structural properties of $CrSi_2$, $MoSi_2$, and WSi_2

L. F. Mattheiss
AT&T Bell Laboratories, Murray Hill, New Jersey 07974
(Received 12 September 1991)

The linear augmented-plane-wave method has been applied to calculate the valence-electron contribution to the total energy of the hexagonal ($C40$) and tetragonal ($C11_b$) phases of the group-VI transition-metal disilicides $CrSi_2$, $MoSi_2$, and WSi_2 in the local-density approximation (LDA). In agreement with experiment, the results show that the tetragonal $C11_b$ phase is the lower-energy structure for both $MoSi_2$ and WSi_2 (by 0.11 and 0.22 eV/formula unit, respectively). However, the LDA fails to replicate the observed switch to the stable hexagonal $C40$ phase in $CrSi_2$, leaving a reduced but positive $C40$-$C11_b$ structural-energy difference of 0.05 eV/formula unit. The calculated lattice parameters for the observed stable phases are in excellent agreement (~ 0.01–0.03 Å) with measured values. Somewhat large discrepancies (~ 0.1–0.3 Å) are found for the c lattice parameters of the metastable hexagonal $MoSi_2$ and WSi_2 compounds.

The refractory disilicides RSi_2 (i.e., those containing groups IV-VI transition-metal constituents R) have found important technological applications in silicon-based microelectronics because of their high-temperature stability and generally low electrical resistivities.[1,2] While these compounds form with a variety of seemingly complicated low-symmetry orthorhombic ($C54$,$C49$), hexagonal ($C40$), and tetragonal ($C11_b$) structures, they do in fact share a common structural building block that consists of nearly hexagonal RSi_2 layers.[3] In particular, the orthorhombic $C54$, hexagonal $C40$, and tetragonal $C11_b$ phases can be generated by introducing simple variations in the stacking sequence of these nearly hexagonal RSi_2 layers. The orthorhombic $C49$ structure is similar, but involves a different registry between layers.

These structural systematics seem to be related to the d-band filling of the transition-metal constituents. For example, the group-IV disilicides form with the orthorhombic $C54$ ($TiSi_2$) or $C49$ ($ZrSi_2$,$HfSi_2$) structures that contain four-layer ($ABCD$) and two-layer (AB') stacking sequences, respectively. On the other hand, the group-V compounds consistently adopt the three-layer (ABC) hexagonal $C40$ structure while the stable phases of the group-VI materials include both the hexagonal $C40$ structure ($CrSi_2$) as well as the two-layer (AB) tetragonal $C11_b$ phase ($MoSi_2$,WSi_2). The transition from hexagonal to tetragonal symmetry among the isoelectronic group-VI compounds suggests a near degeneracy in the structural energies for these phases. This is supported by the fact that metastable hexagonal $MoSi_2$ and WSi_2 thin films can be formed using ion-implantation techniques and low annealing temperatures.[4]

In order to understand theoretically the structural energetics of the group-VI disilicides RSi_2, total-energy calculations have been carried out for the hexagonal and tetragonal phases of these compounds with the use of a scalar-relativistic version of the linear augmented-plane-wave (LAPW) method.[5] Previous studies of these materials have focused primarily on their one-electron band structures, and include results for $CrSi_2$ (Refs. 6–8), $MoSi_2$ (Refs. 8–11), and WSi_2 (Refs. 8, 9, and 12). In addition, the ground-state structural properties of tetragonal $MoSi_2$ have been calculated with the use of the linear-muffin-tin-orbitals (LMTO) method using the atomic-spheres approximation[13] (LMTO-ASA) as well as a full-potential (LMTO-FP) approach.[11] Utilizing the observed lattice parameters for tetragonal $MoSi_2$ and WSi_2, the pseudopotential method has been applied to determine the cohesive energies[9] and heat of formation[14] for these materials. However, there have been no previous studies comparing the $C40$-$C11_b$ structural-energy differences for the three group-VI disilicide compounds $CrSi_2$, $MoSi_2$, and WSi_2. In a preliminary study[7] of $CrSi_2$, a comparison of the LAPW total energies for the $C40$ and $C11_b$ phases with unrelaxed geometries has indicated that the observed hexagonal $C40$ structure may be marginally (~ 0.01 eV/f.u.) more stable.

A complete determination of the hexagonal $C40$ and tetragonal $C11_b$ structures requires the evaluation of three structural parameters, including the a and c lattice parameters as well as an internal Si-atom position parameter x. In the present study, these parameters have been determined sequentially by fixing initially c/a and x at their ideal or observed values and varying the volume to determine the minimum-energy lattice parameter a. Then, subsequent calculations have been carried out in which the c/a ratio and x were successively relaxed to provide a complete determination of the $C40$ and $C11_b$ structural parameters. This process of sequentially determining the $C40$ and $C11_b$ structural parameters is accurate only if the initially chosen values for c/a and x are good estimates of their final relaxed values. This is the case in the present calculations, where relaxation effects decreased the total energies by ~ 2–6×10^{-4} hartree/f.u. for the $C11_b$ results and ~ 0.3–12×10^{-4} hartree/f.u. for the $C40$ structure.

The primitive unit cells for the hexagonal and tetragonal $C11_b$ phases are illustrated in Fig. 1. The $C40$ struc-

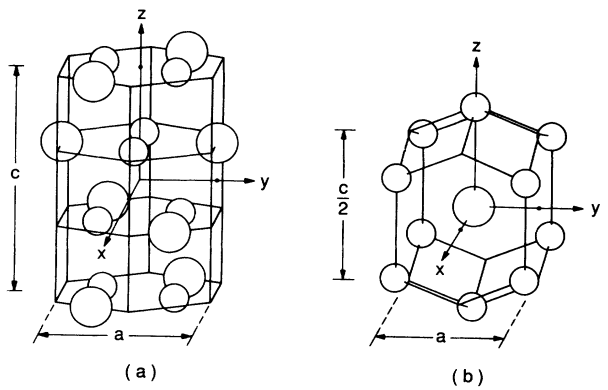

FIG. 1. Primitive unit cells for the (a) hexagonal $C40$ and (b) tetragonal $C11_b$ phases of the group-VI refractory disilicides RSi_2. The R (Si) sites are identified by large (small) spheres.

ture consists of identical nearly hexagonal RSi_2 layers (see Fig. 1 of Ref. 7) which are successively rotated by 60° about the origin, yielding a total of three formula units per primitive cell. The nonsymmorphic $P6_222(D_6^4)$ space group includes nonprimitive translations $\tau=c/3$ and $2c/3$ which restore the lattice by interchanging the individual hexagonal RSi_2 layers. The intralayer R—Si and Si—Si bond distances are determined by the Si-atom position parameter x. These intralayer bond distances are equal for the "ideal" value $x=\frac{1}{6}$. In this case, each R and Si atom has six equidistant coplanar neighbors. The intralayer and interlayer bond distances are also equal for a c/a ratio of 1.5. The observed[2] ratios $c/a\approx 1.39-1.44$ produce interlayer bond distances that are smaller than the corresponding intralayer values.

The corresponding primitive unit cell for the tetragonal $C11_b$ phase contains one RSi_2 formula unit. The symmorphic $I4/mmm(D_{4h}^{17})$ space group is identical to that of the K_2NiF_4 structure, with the R atom occupying the Ni site at the origin and the Si atoms located at the apical F sites. The body-centered-tetragonal Bravais lattice produces the dodecahedral Wigner-Seitz cell shown in Fig. 1(b). In this structure, the sixfold-coordinated nearly hexagonal RSi_2 layers occur in the (110)-type planes and the stacking is AB rather than the ABC sequence of the hexagonal $C40$ structure.

The ideal sixfold coordination at the R- and Si-atom sites in the tetragonal $C11_b$ structure is obtained when $(c/a)_t=\sqrt{6}$ and the Si-atom position parameter $x=\frac{1}{3}$ (see Table III of Ref. 8). For these values, the Si atoms are situated precisely at the vertices of the Wigner-Seitz cell, as shown in Fig. 1. Nearest-neighbor (110) intralayer and interlayer bond distances are equal as a result of tetragonal symmetry. In the limit where the tetragonal and hexagonal structural parameters adopt their "ideal" values [i.e., $(c/a)_t=\sqrt{6}$, $(c/a)_h=\frac{3}{2}$, and $a_t=\sqrt{2}a_h/2$], the unit-cell volumes (per formula unit) for the $C11_b$ and $C40$ phases are equal.

In the present implementation[5] of the LAPW method, a rigid-core approximation is adopted and this facilitates the calculation of the valence-electron contribution to the total energy rather than the total energy itself. These valence electrons include the sd^5 states of Cr, Mo, and W and the $3s^23p^2$ electrons of Si. Both the atomic and LAPW calculations are carried out in a scalar-relativistic approximation which includes all relativistic effects except spin-orbit coupling. The Wigner interpolation formula[15] is applied to treat exchange and correlation effects.

In each of the calculations, the radius of the Si muffin-tin sphere has been fixed at the value $R(\mathrm{Si})\approx 2.07$ a.u. The corresponding transition-metal radii have been set at the somewhat larger values, $R(\mathrm{Cr})\approx 2.39$, $R(\mathrm{Mo})\approx 2.52$, and $R(\mathrm{W})\approx 2.50$ a.u., respectively. These produce nearly touching spheres along the nearest-neighbor bond directions at reduced volumes and help optimize the LAPW convergence. The LAPW basis size has been set using a plane-wave cutoff of 12 Ry. This provides a volume-dependent basis that varies from about 150 to 210 LAPW's per formula unit over the volume range ($\sim$210–295 a.u. per formula unit) of the present investigation. The spherical-harmonic expansion of the LAPW wave functions within the muffin-tin spheres has included terms through $l=6$.

The LAPW calculations impose no shape approximations on either the charge density or the potential. These functions are expanded with $\sim$5000 plane waves (55-Ry cutoff) in the interstitial region and by means of lattice harmonics ($l_{\max}=4$) within the muffin-tin spheres. Brillouin-zone integrations have been carried out with the use of 18 (14) special points in the $\frac{1}{16}$ ($\frac{1}{24}$) irreducible wedge of the tetragonal (hexagonal) Brillouin zone. As shown by the convergence studies described in the Appendix, the present choice of LAPW computational parameters is sufficient for an accurate determination of the structural properties of $CrSi_2$, $MoSi_2$, and WSi_2.

The results of the first-stage structural calculations for $CrSi_2$, $MoSi_2$, and WSi_2 are shown in Figs. 2–4. Here, the valence-electron contribution to the total energies of the $C40$ and $C11_b$ phases of these materials are plotted as functions of volume for fixed values of c/a and x. The triangle symbols denote the calculated LAPW valence-energy results while the solid curves represent cubic or quartic fits to the calculated points. The crosses identify the calculated LAPW energies at the interpolated minimum-energy volume for each phase.

For the tetragonal $C11_b$ calculations, the structural c/a and x(Si) parameters have been fixed at their ideal values, $(c/a)=\sqrt{6}$ and $x(\mathrm{Si})=\frac{1}{3}$. The ideal Si-atom position parameter $x=\frac{1}{6}$ has also been assumed for the $C40$ calculations. Using the experimental results as a guide,[2,4] the $C40$ c/a ratios for these initial-stage calculations have been set at the values 1.44, 1.40, and 1.40 for $CrSi_2$, $MoSi_2$, and WSi_2, respectively.

The results shown in Figs. 2–4 exhibit several interesting features. The first is the fact that for each compound, the minimum-energy volume is nearly identical for both phases. Because of the imposed structural constraints discussed above, this shows that the calculated tetragonal intraplanar R—Si and Si—Si bond distances are smaller in the $C11_b$ phase than the corresponding $C40$ structure.

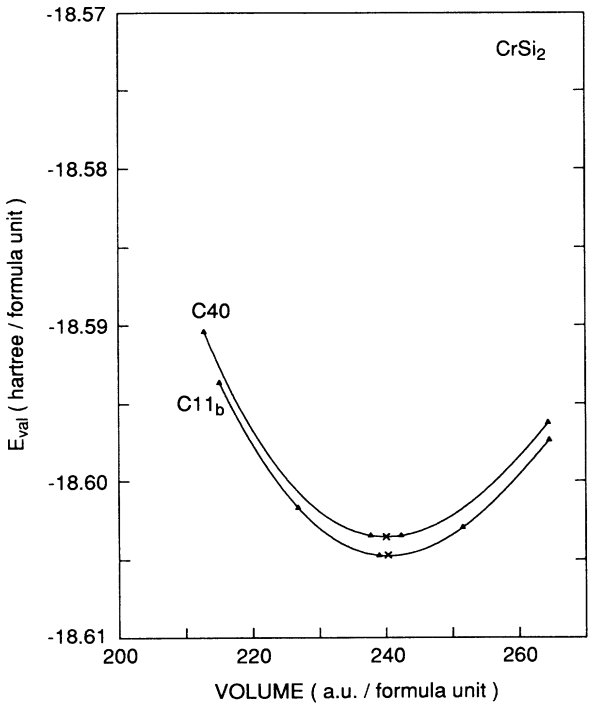

FIG. 2. $CrSi_2$ valence-electron energy E_{val} as a function of volume for the hexagonal $C40$ ($c/a=1.44$, $x=\frac{1}{6}$) and tetragonal $C11_b$ ($c/a=\sqrt{6}$, $x=\frac{1}{3}$) phases with fixed c/a ratios and Si-atom position parameters. The curves are polynomial fits to the calculated LAPW values (triangles). The crosses represent the LAPW energies at the interpolated minimum-energy volume.

The minimum-energy volumes for the two phases agree to within 0.12–0.17 % for $CrSi_2$, $MoSi_2$, and WSi_2.

These results also reflect a monotonic decrease in the structural-energy difference between the $C11_b$ and $C40$ phases. These vary from 0.24 to 0.12 and finally 0.03 eV/f.u. for WSi_2, $MoSi_2$, and $CrSi_2$, respectively. Thus, these partially relaxed LDA results predict that the tetragonal $C11_b$ phase of $CrSi_2$ has a lower total energy than that of the hexagonal $C40$ structure, a result that is contrary to experiment. The volume-dependent $CrSi_2$ results in Fig. 2 provide a simple explanation for the previous findings[7] in which the $CrSi_2C40$ phase was found to be slightly more stable ($\sim$0.01 eV/f.u.) than the tetragonal $C11_b$ structure. Namely, the hexagonal lattice parameters and unit-cell volume ($\sim$241.6 a.u./f.u.) used in this earlier calculation lie close to the minimum energy of the $CrSi_2$ $C40$ curve in Fig. 2 whereas the corresponding (estimated) tetragonal lattice parameters and primitive-cell volume ($\sim$252.3 a.u./f.u.) are found to fall well beyond the calculated $C11_b$ minimum.

In subsequent stages of the present calculations, the c/a ratio and the Si-atom position parameter have been successively relaxed (at the minimum-energy volumes and c/a ratios, respectively), thereby providing a complete determination of the structural parameters for the $C11_b$ and $C40$ phases of $CrSi_2$, $MoSi_2$, and WSi_2. In each case, the LAPW valence-electron energies E_{val} were calculated at incrementally varied $\Delta(c/a)$ and Δx values and the results fitted with a quadratic to determine the minimum. A summary of the calculated results for the Δx variations

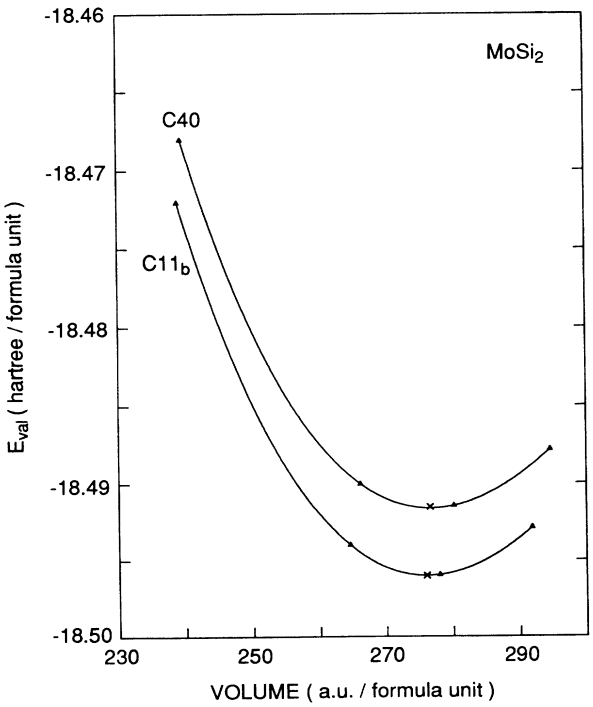

FIG. 3. LAPW valence-energy results for the $C40$ ($c/a=1.40$, $x=\frac{1}{6}$) and $C11_b$ ($c/a=\sqrt{6}$, $x=\frac{1}{3}$) phases of $MoSi_2$, following the notation of Fig. 2.

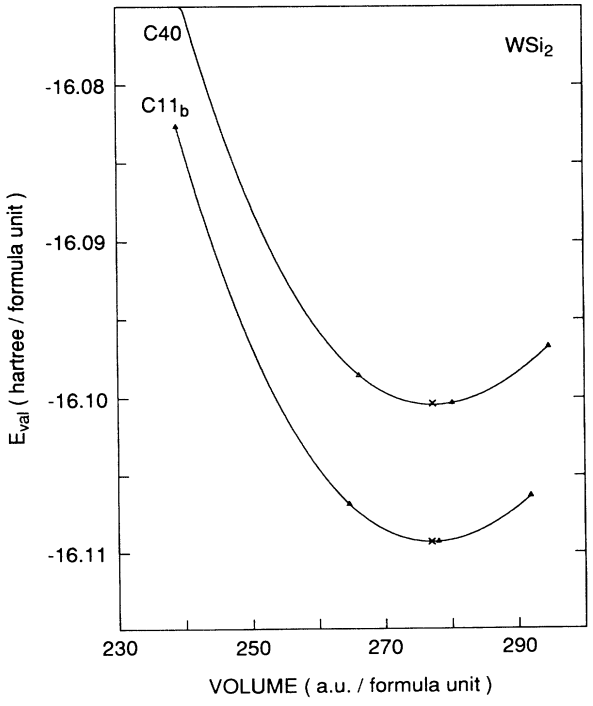

FIG. 4. LAPW valence-energy results for the $C40$ ($c/a=1.40$, $x=\frac{1}{6}$) and $C11_b$ ($c/a=\sqrt{6}$, $x=\frac{1}{3}$) phases of WSi_2, following the notation of Fig. 2.

TABLE I. Summary of calculated (LAPW) and observed (Expt.) structural properties for the tetragonal $C11_b$ and hexagonal $C40$ phases of $CrSi_2$, $MoSi_2$, and WSi_2. For the $C40$ results, $\Omega' \equiv \Omega/3$ represents the cell volume/f.u.

Property	$CrSi_2$ LAPW	$CrSi_2$ Expt.[a]	$MoSi_2$ LAPW	$MoSi_2$ Expt.[a]	WSi_2 LAPW	WSi_2 Expt.[a]
$C11_b$						
a (Å)	3.085		3.222	3.200	3.230	3.212
c (Å)	7.485		7.883	7.861	7.867	7.880
c/a	2.426		2.447	2.457	2.436	2.453
$\Omega = \frac{1}{2}a^2c$ (Å^3)	35.62		40.92	40.25	41.04	40.65
x	0.3368		0.3355		0.3351	
B (Mbar)	2.2[b]		2.3[b]		2.4[b]	
$C40$						
a (Å)	4.397	4.428	4.622	4.605	4.618	4.614
c (Å)	6.374	6.363	6.646	6.559	6.674	6.414
c/a	1.450	1.437	1.438	1.424	1.445	1.390
$\Omega' = \sqrt{3}a^2c/6$ (Å^3)	35.57	36.02	40.99	40.15	41.09	39.42
x	0.1668		0.1642		0.1640	
B (Mbar)	2.1[b]		2.2[b]		2.7[b]	

[a]Reference 2.

[b]Upper-limit estimates from unrelaxed calculations with fixed values of c/a and x.

is shown in Fig. 5. In each case, the minimum-energy geometry produces small shifts from the ideal Si-atom position parameter x(Si) which alters slightly the sixfold planar coordination of the nearly hexagonal RSi_2 layers. In agreement with earlier results,[7,8] these deviations are extremely small ($\Delta x \approx 1.7 \times 10^{-4}$) for hexagonal $CrSi_2$.

The calculated structural parameters for $CrSi_2$, $MoSi_2$, and WSi_2 are summarized and compared with the available experimental values in Table I. As indicated, the calculated lattice parameters for the observed stable phases are consistently in excellent agreement ($\sim$0.03 Å) with the measured values. The deviations are notably larger for the c lattice parameters of the metastable $C40$ $MoSi_2$ ($\sim$0.1 Å) and WSi_2 ($\sim$0.26 Å) phases. The calculated c/a ratios for the tetragonal $C11_b$ phase are consistently smaller than the ideal value, $(c/a)_{\text{ideal}} = \sqrt{6} \approx 2.4495$, whereas the measured values for $MoSi_2$ and WSi_2 are slightly larger. The calculated bulk moduli indicate a comparable stiffness for the two phases and a gradual increase for the $4d$ and $5d$ compounds.

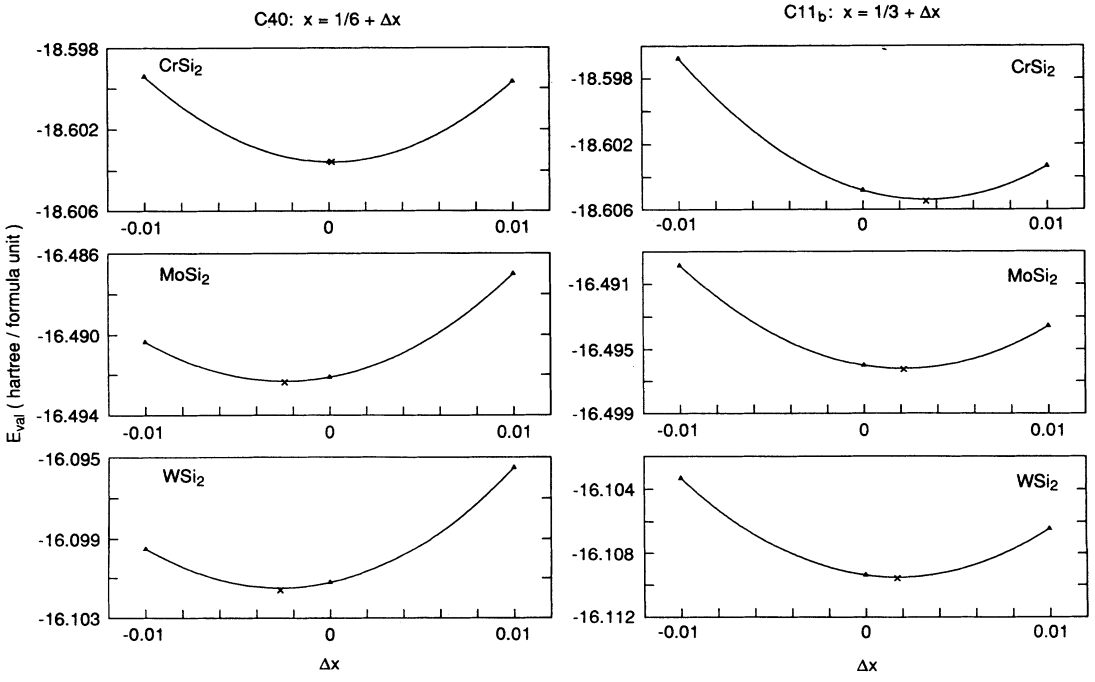

FIG. 5. Calculated dependence of the valence energies E_{val} for $CrSi_2$, $MoSi_2$, and WSi_2 on the Si-atom position parameter x(Si).

TABLE II. Comparison of fully relaxed LAPW valence-band energies E_{val} (hartree/f.u.) for the $C40$ and $C11_b$ phases of $CrSi_2$, $MoSi_2$, and WSi_2. The $C40$-$C11_b$ energy difference is given by ΔE_{val} (eV/f.u.). Calculated and observed heats of formation H_b (eV/f.u.) for the group-VI disilicides.

	$CrSi_2$	$MoSi_2$	WSi_2
$E_{val}(C40)$	−18.603 57	−16.492 37	−16.101 60
$E_{val}(C11_b)$	−18.605 51	−16.496 27	−16.109 58
ΔE_{val}	0.05	0.11	0.22
H_f: LAPW[a] (Expt.)			
$C40$	1.02 (1.27)[b]	1.34	0.80
$C11_b$	1.07	1.45(1.13)[b]	1.02(0.96)[b]
		(1.18,1.36)[c]	(0.97)[c]

[a]Evaluated using the Si valence-electron energies of Ref. 16 and the Cr, Mo, and W results of Ref. 5.
[b]Reference 17.
[c]Reference 18.

The fully relaxed valence-energy results for the $C40$ and $C11_b$ phases of the group-VI RSi_2 compounds are summarized in Table II. It is found that while the $C40$-$C11_b$ valence-energy differences (ΔE_{val}) for $MoSi_2$ and WSi_2 have decreased slightly ($\sim$0.01–0.02 eV/f.u.) as a result of relaxation effects, the corresponding $CrSi_2$ value for ΔE_{val} has increased from $\sim$0.03 to 0.05 eV/f.u. According to convergence studies, which are discussed in the Appendix, this LDA prediction that the tetragonal $C11_b$ phase of $CrSi_2$ is more stable than the observed $C40$ structure is unaffected by changes in LAPW computational parameters and cutoffs. Thus, it is concluded that LDA fails to predict the correct ground-state structure of $CrSi_2$.

Combining the $E_{val}(C40)$ and $E_{val}(C11_b)$ results of Table II with previous LAPW valence-energy results for Si (Ref. 16) and Cr, Mo, and W (Ref. 5) permits the calculation of the heats of formation H_f for the group-VI disilicides. As shown in the lower portion of Table II, these results are in reasonable accord with measured values.

As mentioned earlier, there have been several independent calculations of the structural properties of tetragonal $MoSi_2$ involving a variety of computational techniques. These results are compared with the present LAPW calculations and experiment in Table III. In general, the overall agreement between the various calculated results and experiment is excellent. The LAPW lattice parameters are slightly larger than the experimental values, while the LMTO results are somewhat smaller. The individual calculated values for the cohesive energies E_{coh} agree to within $\sim$1.5% but are consistently $\sim$15% larger than experiment. The LAPW heat of formation H_f is about 20% smaller than the LMTO-FP and pseudopotential values and is within 1% of the largest experimental value.

One can determine the frequency of the zone-center fully symmetric (A_{1g}) optical-phonon mode from the curvature of E_{val} versus Δx at the energy minima in Fig. 5. In Table IV, the present LAPW values of x(Si) and ν(Si) are compared with those of previous calculations[9,11] and the results of recent Raman measurements[19] of optical-phonon frequencies in both hexagonal and tetragonal $MoSi_2$. The LAPW Si-atom position parameters x(Si) are consistently smaller than the corresponding pseudopotential values[9] for $MoSi_2$ and WSi_2. The same is true for the A_{1g} phonon frequencies. The present calculated A_{1g} frequency for tetragonal $MoSi_2$ is in good agreement with the Raman value,[19] provided that the authors' assignment of the A_{1g}(325 cm^{-1}) and E_g(440 cm^{-1}) modes is reversed. It is noted that this reassignment is consistent with the interpretation[20] of Raman spectra for La_2CuO_4, where the Si and apical O atoms occupy the same crystallographic sites in the tetragonal unit cell.

TABLE III. Comparison between the observed structural properties for tetragonal $MoSi_2$ and those determined in the present LAPW calculation as well as earlier LMTO-FP (Ref. 11), LMTO-ASA (Ref. 13), and pseudopotential (Refs. 9 and 14) investigations. The values for the cohesive energy (E_{coh}) and heats of formation (H_f) are in eV/f.u.

Method	a (Å)	c (Å)	B (Mbar)	E_{coh}	H_f
Expt.	3.200[a]	7.861[a]		16.90[b]	1.13[c]
					1.18,1.36[d]
LAPW	3.222	7.883	2.3	19.26	1.45
LMTO-FP	3.186	7.800	2.22	19.15	1.87
LMTO-ASA	3.189	7.821	2.38		
Pseudo				19.69	1.78

[a]Reference 2.
[b]Reference 11.
[c]Reference 17.
[d]Reference 18.

TABLE IV. Calculated and observed values for the Si-atom position parameters x(Si) and the corresponding fully symmetric (A_{1g}) optical phonon frequencies ν(Si).

	$CrSi_2$		$MoSi_2$		WSi_2	
	$C11_b$	$C40$	$C11_b$	$C40$	$C11_b$	$C40$
x(Si)						
LAPW[a]	0.3368	0.1668	0.3355	0.1642	0.3351	0.1640
Pseudo[b]			0.3374		0.3366	
LMTO-FP[c]			0.3333			
ν(Si) (cm^{-1})						
LAPW[a]	473	428	427	376	438	391
Pseudo[b]			478		493	
Expt.[d]			440[e]	395[f]		
				420[f]		

[a]Present work.
[b]Reference 9.
[c]Reference 11.
[d]Reference 19.
[e]The authors' assignment of the A_{1g} (325 cm^{-1}) and E_g (440 cm^{-1}) modes is reversed here on the grounds that the bond-stretching (A_{1g}) mode should have the higher frequency.
[f]These represent two strong unassigned high-frequency modes for the $C40$ phase.

As shown in previous studies,[7,8] hexagonal $CrSi_2$ is an indirect-gap semiconductor with a valence-band maximum at the L point in the Brillouin zone and conduction-band minima at M. The calculated gap of 0.30 eV is in excellent agreement with the measured[21] optical gap of 0.35 eV. Changes in the position and width of the Mo($4d$) and W($5d$) bands relative to the Cr($3d$) bands and E_F in $CrSi_2$ lead to reduced gaps of 0.02 and -0.03 eV for the metastable $C40$ phases of $MoSi_2$ and WSi_2, respectively. Based on previous calculations,[7,9–12] metallic behavior is expected for the entire family of tetragonal group-VI disilicides. In view of the sensitivity of the calculated $CrSi_2$ gap to structural and chemical variations,[7] it is informative to trace the evolution of this gap (i.e., its dependence on volume, c/a ratio, and x) in the present calculations for the hexagonal group-VI disilicides.

The calculated variation of the $C40$ $CrSi_2$, $MoSi_2$, and WSi_2 indirect band gap E_{gap} with volume, c/a ratio, and Si-atom position parameter x is shown in Fig. 6. A striking difference between $CrSi_2$ and its $4d$-$5d$ counterparts is illustrated by the gap dependence on volume. As shown in the leftmost panel, the $CrSi_2$ indirect gap decreases with increasing volume whereas the corresponding $MoSi_2$ and WSi_2 gaps increase. All three materials exhibit a similar dependence of E_{gap} on c/a and x. The final calculated gaps for the fully relaxed geometries are $E_{gap}(CrSi_2)=0.302$ eV, $E_{gap}(MoSi_2)=0.035$ eV, and $E_{gap}(WSi_2)=-0.003$ eV, which are all slightly larger than the values obtained previously using measured values for the lattice parameters.[8]

The structural similarities between the hexagonal $C40$ and tetragonal $C11_b$ phases of the group-VI disilicides are also reflected in their one-electron band properties at energies well removed from the Fermi level. A global view of these similarities is provided in Fig. 7 by the density-of-states (DOS) results for the $C11_b$ and $C40$ phases of $CrSi_2$, $MoSi_2$, and WSi_2 at their minimum-energy geometries. These DOS curves have been calculated with the use of tetrahedral interpolation based on 21 (60) **k** points in the irreducible wedge of the hexagonal (tetragonal) Brillouin zone. In each material, the dashed transition-metal d-band component is enhanced near the Fermi level. The $C11_b$ results exhibit a DOS minimum near E_F with a pseudogap separating the filled and unoccupied d bands. Rather similar DOS structure is exhibited by the $C40$ results, though in this case the DOS goes to zero at E_F. Note that the overall valence bandwidth is consistently $\sim$14 eV and is slightly larger ($\sim$0.3 eV) for the $C40$ phase. The "peaky" structure of the $C40$ DOS results is due in part to the presence of three RSi_2 formula units per primitive cell and the corresponding three-

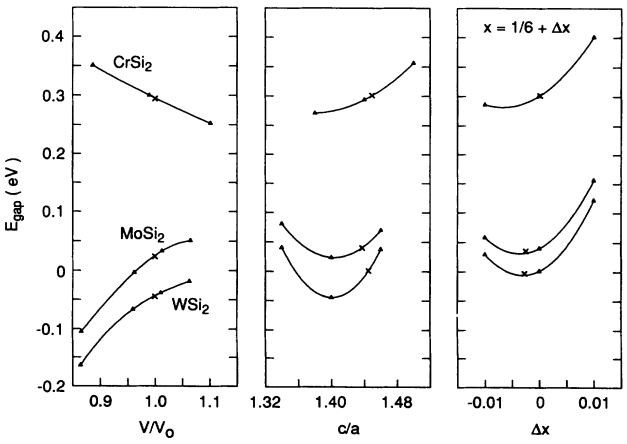

FIG. 6. Calculated dependence of the indirect band gap of hexagonal $CrSi_2$, $MoSi_2$, and WSi_2 on volume, c/a ratio, and the Si-atom position parameter x(Si).

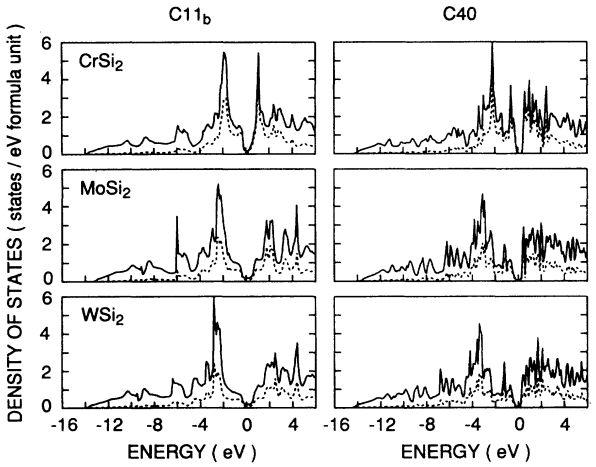

FIG. 7. Comparison of LAPW density-of-states results for the $C11_b$ and $C40$ phases of $CrSi_2$, $MoSi_2$, and WSi_2. The projected transition-element component is shown by the dashed curves.

fold increase in the number of valence bands.

In addition, one expects very similar bonding characteristics for these group-VI disilicides, particularly within the nearly hexagonal RSi_2 layers that underlie the hexagonal and tetragonal structures of these materials. The LAPW valence-electron charge densities in the (110) and (0001) planes of the $C11_b$ and $C40$ structures are compared in Fig. 8. In general, the magnitude and shape of the charge-density contours surrounding the R- and Si-atom sites are quite similar in these compounds. A subtle difference between the tetragonal and hexagonal results is produced by slight variations in the d-band occupancy. This causes nonspherical deviations of the R-atom d-band charge that is localized around these sites (i.e., the center and corners of each plot). In the tetragonal $C11_b$ results, these deviations reflect enhanced bonding along [110] directions; the corresponding bonds are rotated by 90° in the $C40$ phase. The orientation of the present $C40$ results is such that primitive-cell origins are located midway along the vertical edges. Taking this into account, the $C40$ $CrSi_2$ valence-electron charge-density results are in good agreement with those calculated using the observed lattice parameters.[8] Similar agreement is found between the present LAPW charge densities for tetragonal $MoSi_2$ and WSi_2 and the fully relativistic pseudopotential results ($MoSi_2$ and WSi_2) of Bhattacharyya, Bylander, and Kleinman[9] and the LMTO-FP results ($MoSi_2$) of Alouani, Albers, and Methfessel.[11] However, the nonspherical charge distribution at the Mo site is visibly diminished in the latter results.

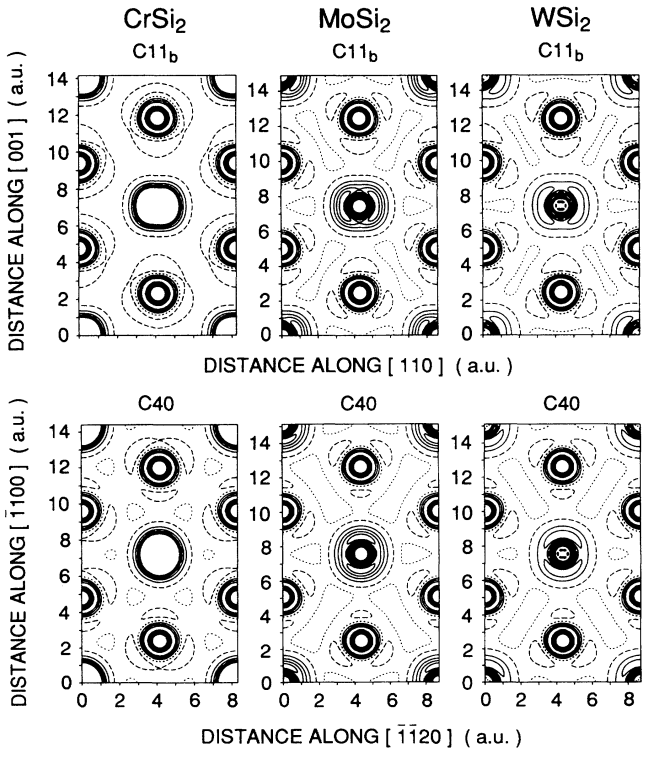

FIG. 8. LAPW valence-electron charge-density contours in the nearly hexagonal planes of the $C11_b$ and $C40$ structures. The contour interval is 0.012 (0.024) electrons/a_B^3 below (above) the 0.060 electrons/a_B^3 value that is identified by the long-dashed curves. The short-dashed curves label the contour value 0.048 electrons/a_B^3.

In summary, the structural properties and relative stability of the hexagonal $C40$ and tetragonal $C11_b$ phases of $CrSi_2$, $MoSi_2$, and WSi_2 have been studied by means of LAPW total-energy LDA calculations. These calculations predict that the tetragonal $C11_b$ phase is the lowest-energy structure for the entire family of group-VI disilicides, with $C40$-$C11_b$ energy differences of 0.05, 0.11, and 0.22 eV/f.u. for $CrSi_2$, $MoSi_2$, and WSi_2, respectively. The $CrSi_2$ result is at odds with experiment since the observed stable structure is the hexagonal $C40$ rather than the tetragonal $C11_b$ phase. In all cases, the calculated structural parameters for the actual stable phases are in good agreement with experiment. The present results suggest that it should be possible to prepare a metastable tetragonal form of $CrSi_2$. The calculated $CrSi_2$ $C40$-$C11_b$ structural-energy difference is much smaller than that for $MoSi_2$ and WSi_2, where the metastable $C40$ phase has been successfully produced in appropriately treated thin-film samples.[4]

APPENDIX

Because the LAPW structural-energy difference between the $CrSi_2$ $C40$ and $C11_b$ phases is quite small ($\sim 2\times 10^{-3}$ hartree/f.u.), it is important to determine the extent to which this result is affected by variations in individual LAPW computational parameters. In this appendix, we discuss supplementary calculations for hexagonal and tetragonal $CrSi_2$ in which the effects of increased basis size, improved Brillouin-zone integrations, and extended LAPW cutoff parameters are assessed.

This study has focused on the first-stage $CrSi_2$ results of Fig. 2 at the designated $C40$ and $C11_b$ volumes (237.69 and 238.96 a.u./f.u., respectively) which are slightly smaller than the minimum-energy values. The calculated $C40$-$C11_b$ energy difference at these volumes ($\sim 1.28 \times 10^{-3}$ hartree/f.u.) mirrors that at the energy minima ($\sim 1.17 \times 10^{-3}$ hartree/f.u.). In these test calculations (i) the spherical-harmonic expansion of the LAPW wave functions inside the spheres has been increased from $l=6$ to 8; (ii) the plane-wave cutoff for the interstitial charge-density and potential expansion has been increased from 55 to 75 Ry; (iii) the lattice-harmonic expansion inside the spheres has been increased from $l_{max}=4$ to 5 ($C40$) or $l_{max}=6$ ($C11_b$). LAPW calculations incorporating these modified cutoffs have yielded results in which the $CrSi_2$ $C40$-$C11_b$ energy difference increased from $\sim 1.28 \times 10^{-3}$ to $\sim 1.35 \times 10^{-3}$ hartree/f.u.

A second aspect of these comparative studies focused on the relative convergence of the $C40$ and $C11_b$ valence energies as a function of basis size. The results of this study are summarized in Fig. 9, where the calculated $C40$ and $C11_b$ valence energies E_{val} are plotted as functions of $(k_c R)^{-11}$, where k_c^2 is the plane-wave kinetic-energy cutoff (in Ry) and $R \approx 2.39$ a.u. is the Cr muffin-tin sphere radius. The tetragonal $C11_b$ results for $k_c^2=12$, 14, 16, and 18 Ry are well described by a straight line. The corresponding $C40$ results for $k_c^2=12$ and 14 Ry lie on a parallel straight line. In both cases, deviations are evident for the lower-cutoff results ($k_c^2=10$ Ry) which are shown to the far right in the figure. The extrapolated intercepts suggest that the $C40$-$C11_b$ energy difference at $k_c^2=12$ Ry (triangle symbols) is maintained in the fully converged limit.

Further tests have shown that improved Brillouin-zone sampling for the $C11_b$ (30 versus 18 **k** points) and $C40$ (24 vs 14 **k** points) at the $k_c^2=12$ Ry cutoff also preserves this $C40$-$C11_b$ energy difference in the $\sim 1.2 \times 10^{-3}$ hartree/f.u. range. Thus, based on these convergence studies, it is concluded that the LDA fails to predict that the $C40$ phase of $CrSi_2$ has a lower energy than the tetragonal $C11_b$ structure.

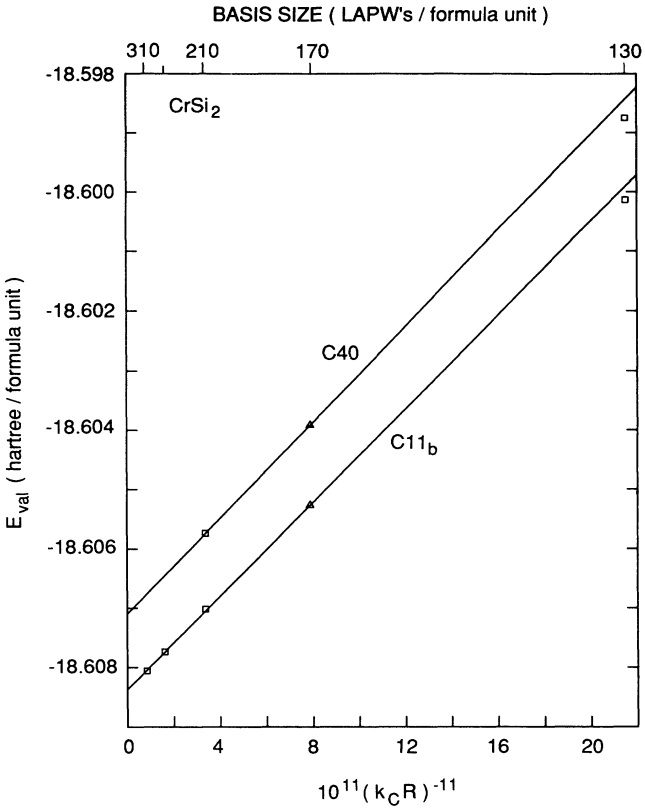

FIG. 9. Calculated LAPW valence-energy results for the $C40$ and $C11_b$ phases of $CrSi_2$ as a function of $(k_c R)^{-11}$, where $R \approx 2.39$ a.u. is the Cr muffin-tin-sphere radius and k_c^2 is the LAPW-basis cutoff parameter.

[1] S. P. Murarka, J. Vac. Sci. Technol. **17**, 775 (1980).

[2] M.-A. Nicolet and S. S. Lau, in *VLSI Electronics: Microstructure Science,* edited by N. G. Einspruch and G. B. Larrabee (Academic, New York, 1983), Vol. 6, p. 329.

[3] F. Laves, in *Theory of Alloy Phases* (American Society for Metals, Metal Park, OH, 1956), p. 181.

[4] F. M. d'Heurle, C. Petersson, and M. Y. Tsai, J. Appl. Phys. **51**, 5976 (1980).

[5] L. F. Mattheiss and D. R. Hamann, Phys. Rev. B **33**, 823 (1986); O. K. Andersen, *ibid.* **12**, 3060 (1975).

[6] A. Franciosi, J. H. Weaver, D. G. O'Neill, F. A. Schmidt, O. Bisi, and C. Calandra, Phys. Rev. B **28**, 7000 (1983).

[7] L. F. Mattheiss, Phys. Rev. B **43**, 1863 (1991).

[8] L. F. Mattheiss, Phys. Rev. B **43**, 12 549 (1991).

[9] B. K. Bhattacharyya, D. M. Bylander, and L. Kleinman, Phys. Rev. B **32**, 7973 (1985).

[10] S. Tang and K. Zhang, J. Phys. C **21**, 1469 (1988).

[11] M. Alouani, R. C. Albers, and M. Methfessel, Phys. Rev. B **43**, 6500 (1991).

[12] B. K. Bhattacharyya, D. M. Bylander, and L. Kleinman, Phys. Rev. B **31**, 2049 (1985); **31**, 5462 (1985).

[13] S. Tang, K. Zhang, and X. Xie, J. Phys. C **21**, L777 (1988).

[14] M. J. Zhu, D. M. Bylander, and L. Kleinman, Phys. Rev. B **36**, 3182 (1987).

[15] E. Wigner, Phys. Rev. **46**, 1002 (1934).

[16] D. R. Hamann and L. F. Mattheiss, Phys. Rev. Lett. **54**, 2517 (1985).

[17] G. V. Samsonov and I. M. Vinitskii, *Handbook of Refractory Compounds* (Plenum, New York, 1980).

[18] H. J. Goldschmidt, *Interstitial Alloys* (Plenum, New York, 1967).

[19] C. M. Doland and R. J. Nemanich, J. Mater. Res. **5**, 2854 (1990).

[20] S. Blumenroeder, E. Zirngiebl, J. D. Thompson, P. Killough, J. L. Smith, and Z. Fisk, Phys. Rev. B **35**, 8840 (1987); W. H. Weber, C. R. Peters, B. M. Wanklyn, C. Chen, and B. E. Watts, *ibid.* **38**, 917 (1988).

[21] M. C. Bost and J. E. Mahan, J. Appl. Phys. **63**, 839 (1988).